Research Article | Vol. 26, No. 21 | 15 Oct 2018 | OPTICS EXPRESS 27978
Optics EXPRESS

Nonlinear frequency division multiplexing with b-modulation: shifting the energy barrier

TAO GUI,[1,4] GAI ZHOU,[1] CHAO LU,[2] ALAN PAK TAO LAU,[1] AND SANDER WAHLS[3,5]

[1]*Photonics Research Centre, Department of Electrical Engineering, The Hong Kong Polytechnic University, Hung Hom, Kowloon, Hong Kong*
[2]*Photonics Research Centre, Department of Electronic and Information Engineering, The Hong Kong Polytechnic University, Hung Hom, Kowloon, Hong Kong*
[3]*Delft Center for Systems and Control, Delft University of Technology, Mekelweg 2, 2628 CD Delft, The Netherlands*
[4]*tao.gui@connect.polyu.hk*
[5]*s.wahls@tudelft.nl*

Abstract: The recently proposed b-modulation method for nonlinear Fourier transform-based fiber-optic transmission offers explicit control over the duration of the generated pulses and therewith solves a longstanding practical problem. The currently used b-modulation however suffers from a fundamental energy barrier. There is a limit to the energy of the pulses, in normalized units, that can be generated. In this paper, we discuss how the energy barrier can be shifted by proper design of the carrier waveform and the modulation alphabet. In an experiment, it is found that the improved b-modulator achieves both a higher Q-factor and a further reach than a comparable conventional b-modulator. Furthermore, it performs significantly better than conventional approaches that modulate the reflection coefficient.

1. Introduction

Nonlinear impairments are a major limiting factor in fiber-optic data transmission. There has been significant interest in utilizing the nonlinear Fourier transform (NFT) for data transmission in the last few years [1–7]. The NFT decomposes the ideal Nonlinear Schrödinger Equation (NLS) into a set of parallel communication channels characterized by a nonlinear spectrum [8]. The propagation of signals encoded under this framework reduces, similar to linear channels in the conventional frequency domain, to a simple multiplication with a transfer function. The nonlinear spectrum is divided into two parts: the continuous spectrum, which depends on a real parameter ξ (corresponding to the "dispersive" signal components), and the discrete spectrum where eigenvalues λ lie in the upper half of the complex plane (corresponding to the "solitonic" signal components). Exploiting nonlinearity in optical systems started two decades ago with on-off keying soliton transmissions. A form of 'eigenvalue communication' was first proposed in [9]. Following the advances of digital coherent technology in the last decade, arbitrarily complex phase and amplitude modulated signals can be generated and received. Thus, today more dimensions can be used in NFT-based communication designs. Numerous proof-of-concept experiments have been demonstrated by many groups during the last few years. With the modulation of the discrete part (eigenvalue transmission), data rates up to 24 Gbps at 4 Gbaud (6 bits/symbol) have been reported [10]. By modulating the continuous part only, 32 Gb/s transmission with 64 modulated nonlinear subcarriers was demonstrated over 1464 km in [11], showing over 1 dB performance advantage over conventional frequency division multiplexed (FDM) transmissions. The first system modulating both discrete and continuous modes at 26.3 Gbps has been demonstrated in [12].

However, a current issue in NFT-based transmission is that most modulation methods (i.e., methods to embed blocks of data in a nonlinear Fourier spectrum) do not offer tight

#338240 https://doi.org/10.1364/OE.26.027978
Journal © 2018 Received 9 Jul 2018; revised 24 Aug 2018; accepted 6 Sep 2018; published 10 Oct 2018

Optics EXPRESS

control over the duration of the pulse. One solution to this problem is to use the NFT for periodic signals instead of the more common NFT for vanishing signals [13–15]. The transmitter only transmits one period of the generated signal plus a cyclic prefix in this scenario, similar to conventional OFDM. The challenge of the periodic NFT approach is that the NFT for periodic signals is mathematically more complicated. It is in particular not straight-forward to enforce a desired period. So far, only relatively simple systems with a few degrees of freedom have been demonstrated. An alternative solution is our proposed b-modulation method [16], which is based on the NFT for vanishing signals and can generate pulses of a finite, pre-specified duration in a simple way. This method was adopted in an experimental demonstration of 100 Gbps b-modulated nonlinear frequency division multiplexed (NFDM) transmission using 132 subcarriers [17]. A dual polarization NFDM transmission achieving a record net data rate of 400 Gbps based on b-modulation was demonstrated in [18].

In this paper, we extend our previous work [16] and add several modifications to the original b-modulation scheme, including flat top carriers and constellation shaping. The modified method is numerally studied to show the advantages of limited signal time duration compared with conventional modulation of the continuous spectrum ($\hat{q}$ -modulation). In a back-to-back (B2B) scenario, simulation results show that signal-noise interactions through NFT-processing can be significantly reduced for improved b-modulated signals. Based on the results, we experimentally compare the modified b-modulator techniques with conventional b- and $\hat{q}$ -modulation schemes for a 14.4 Gbps 16QAM NFDM transmission over 640km standard single-mode fiber (SSMF). The proposed b-modulation scheme demonstrates a *Q*-factor gain of ~1.2 dB and nonlinear tolerance (launched power) gain of ~4 dB over a conventional FDM system. The results serve as another step forward in designing high performance NDFM signaling techniques for nonlinear transmission systems.

2. Introduction to the b-modulation method

2.1 Basics of the nonlinear Fourier transform

The NFT of a signal $q(t)$, which in our context is either the (normalized) input to or the (normalized) output of a single-mode fiber with anomalous dispersion, is defined in a two-step procedure. First, consider the Zakharov-Shabat problem (see, e.g., [8]) z

$$\frac{\mathrm{d}}{\mathrm{dt}}\begin{bmatrix}\phi_1(t;\lambda)\\ \phi_2(t;\lambda)\end{bmatrix}=\begin{bmatrix}-j\lambda & q(t)\\ -q^*(t) & j\lambda\end{bmatrix}\begin{bmatrix}\phi_1(t;\lambda)\\ \phi_2(t;\lambda)\end{bmatrix},\begin{bmatrix}a(t;\lambda)\\ b(t;\lambda)\end{bmatrix}:=\begin{bmatrix}e^{j\lambda t}\phi_1(t;\lambda)\\ e^{-j\lambda t}\phi_2(t;\lambda)\end{bmatrix}\overset{t\to-\infty}{\to}\begin{bmatrix}1\\0\end{bmatrix}, \quad (1)$$

where λ is parameter. The NFT of $q(t)$ has two parts defined in terms of the limits $a(\lambda):=a(\infty;\lambda)$ and $b(\lambda):=b(\infty;\lambda)$. The first part is the continuous spectrum $\hat{q}(\xi):=b(\xi)/a(\xi)$, where $\xi\in\mathbb{R}$. The second part is the discrete spectrum $(\lambda_k,\rho_k)_{k=1}^{K}$, where the eigenvalues λ_k are the solutions to $a(\lambda)=0$ in $\Im\lambda>0$, and the residues are given by $\rho_k:=b(\lambda_k)/\frac{da}{d\lambda}(\lambda_k)$.

The main advantage of the NFT is that it simplifies the nonlinear Schrödinger equation

$$j\frac{\partial u}{\partial z}=\frac{\partial^2 u}{\partial t^2}+2u|u|^2, \quad u=u(z,t), \quad (2)$$

Optics EXPRESS

which models the evolution of the complex envelope $u(z,t)$ at location z and at retarded time t in an ideal optical fiber. Denoting the functions $a(\lambda)$ and $b(\lambda)$ that correspond to the signal $q(t)=u(z,t)$ by $a_z(\lambda)$ and $b_z(\lambda)$ respectively, the NFT of the fiber input $u(0,t)$ can be reconstructed from the NFT of the fiber output $u(z,t)$ using the relations

$$a_z(\xi)=a_0(\xi),\ b_z(\xi)=e^{-4j\xi^2 z}b_0(\xi). \tag{3}$$

2.2 Conventional modulation methods for the continuous spectrum

We first aim to embed data in the continuous spectrum of the fiber input. The discrete spectrum is not used and chosen to be empty. Several methods have been proposed to modulate a block of symbols $s_{-N},\ldots,s_N \in \mathcal{A}$, where $\mathcal{A}$ is a finite modulation alphabet, into the continuous spectrum. Let $\psi(\xi)$ denote a carrier waveform, $A>0$ a power control factor, and $\xi_s>0$ a shift. Most modulation methods (e.g., [3, 19]) for $\hat{q}(\xi)$ take one of two forms,

$$\hat{q}_1(\xi) := Au(\xi) \quad \text{or} \quad \hat{q}_2(\xi) := \sqrt{e^{A^2|u(\xi)|^2}-1}\,e^{j\angle u(\xi)}, \tag{4}$$

where the power control factor $A>0$ is a constant and

$$u(\xi) := \sum_{n=-N}^{N} s_n \psi(\xi - n\xi_s). \tag{5}$$

2.3 The original b-modulation method

The conventional modulation methods for the continuous spectrum offer no control over the duration of the fiber input and suffer from poor utilization of the temporal domain. Motivated by a classic result for the NFT with respect to the Korteweg-de Vries equation [24], it was recently proposed to modulate $b(\xi)$ instead of $\hat{q}(\xi)=b(\xi)/a(\xi)$ [16]. The modulation scheme in [16] was of the form

$$b(\xi)=Au(\xi), \qquad \text{with } A \text{ and } u(\xi) \text{ as defined above.} \tag{6}$$

It was observed that the generated fiber-input $q(t)$ would be time-limited with

$$q(t)=0 \quad \text{for } t\notin\left[-\frac{T}{2},\frac{T}{2}\right] \tag{7}$$

if the carrier waveform $\psi(\xi)$ was bandlimited in the sense that its conventional inverse Fourier transform

$$\Psi(\tau) := \int_{-\infty}^{\infty} \psi(\xi) e^{j\tau\xi} \frac{d\xi}{2\pi} \tag{8}$$

satisfies $\Psi(\tau)=0$ for $\tau\notin[-T,T]$. Note that this condition is a continuous-time version of the realizability conditions derived in the context of codirectional coupler design [22]: in the absence of eigenvalues, the discrete-time version of $q(t)$ is zero outside a given range if and only if the Fourier series coefficients of the discrete-time version of $b(\xi)$ are zero outside a related range. Also note that it is essential that the power scaling factor is a constant w.r.t. to the nonlinear spectral parameter ξ. Except in very specific special cases, a ξ-dependent

Optics EXPRESS

power control factor will lead to a time-domain signal that is no longer time-limited even if the carrier wave fulfills the condition mentioned above.

The original b-modulation scheme in [16] is one of the first NFT-based modulation method that offers explicit control over the duration of the generated fiber inputs. It has been demonstrated experimentally in [17, 23], where the carrier waveform was a sinc pulse. We also remark that it was recently proposed [21] to embed information in the analytic extension $b(\xi)$ of $\hat{q}(\xi)$, but the methods in [21] do not lead to time-limited signals.

2.4 The energy barrier

The energy $\mathrm{E}:=\int_{-\infty}^{\infty}|q(t)|^2\,dt$ of the generated fiber-input is known to satisfy [8]

$$\mathrm{E}=-\frac{1}{\pi}\int_{-\infty}^{\infty}\log\left(1-|b(\xi)|^2\right)d\xi. \tag{9}$$

On the other hand, it is also known [8] that a valid $b(\xi)$ satisfies $|a(\xi)|^2+|b(\xi)|^2=1$ and thus, in particular,

$$|b(\xi)|<1 \quad \textit{for all}\ \xi. \tag{10}$$

It was observed in [16] that even if the power control factor A is driven towards the limit imposed by the condition $|b(\xi)|=\mathrm{A}|\mathrm{u}(\xi)|<1$, the energy of the generated pulses would not surpass a certain finite limit. To better understand this phenomenon, let us consider the case of a single carrier with a unit symbol, i.e. $b(\xi)=\mathrm{A}\psi(\xi)$. The single carrier case will be indicative for the general case if the shift ξ_s used in the definition of $b(\xi)=\mathrm{A}\mathrm{u}(\xi)$ is large enough. In the single carrier case, the condition $|b(\xi)|<1$ translates into $\mathrm{A}<1/\sup_{\xi}|\psi(\xi)|$. The maximum energy we can achieve by adjusting the power control factor A in this case thus is

$$\mathrm{MCE}[\psi]:=\lim_{\mathrm{A}\to\left(1/\sup_{\xi}|\psi(\xi)|\right)^{-}}-\frac{1}{\pi}\int_{-\infty}^{\infty}\log\left(1-\mathrm{A}^2|\psi(\xi)|^2\right)d\xi \tag{11}$$

We call $\mathrm{MCE}[\psi]$ the *maximum carrier energy* of the carrier waveform $\psi(\xi)$. The MCE can be both finite or infinite, depending on the carrier waveform. Consider, e.g.,

$$\psi_{example}(\xi)=\begin{cases}\sqrt{1-\xi^{2n}}, & if\ |\xi|\le 1\\ 0, & if\ |\xi|>1\end{cases},\qquad n\in\{1,2,3,\ldots\}. \tag{12}$$

The MCE of this carrier waveform is finite for any value of n,

$$\mathrm{MCE}\left[\psi_{example}\right]=\lim_{\mathrm{A}\to 1^{-}}-\frac{1}{\pi}\int_{-1}^{1}\log\left(1-\mathrm{A}^2\left(1-\xi^{2n}\right)\right)d\xi=-\frac{1}{\pi}\int_{-1}^{1}\log\xi^{2n}\,d\xi=\frac{4n}{\pi}<\infty. \tag{13}$$

The carrier waveforms in [16] were impulse responses of raised cosines, and it can be checked numerically that their MCE is indeed finite as well. Interestingly, this is not true for all carrier waveforms. The MCE of a rectangular carrier waveform,

Optics EXPRESS

$$\psi_{rect}(\xi)=\begin{cases}1, \text{ if } |\xi|\le 1\\ 0, \text{ if } |\xi|>1\end{cases} \tag{14}$$

is actually infinite,

$$\mathrm{MCE}[\psi_{rect}]=\lim_{\mathrm{A}\to 1^-}-\frac{1}{\pi}\int_{-1}^{1}\log\left(1-\mathrm{A}^2\right)d\xi=-\frac{2}{\pi}\lim_{A\to 1^-}\log(1-\mathrm{A}^2)=\infty. \tag{15}$$

Rectangular carriers however defeat the purpose of b-modulation – their inverse Fourier transform $\Psi(\tau)$ is not compactly supported, so that the duration of the generated pulses is not finite anymore. The same discussion applies if a root raised cosine is chosen as the carrier $\psi(\xi)$, or if $b(\xi)$ is formed similar to $\hat{q}_2(\xi)$ as in [18]. In both cases, the energy barrier is defeated, but the signals are no longer of finite duration because $b(\xi)$ is not bandlimited.

In contrast, the energy barrier is not that relevant for conventional modulation of the continuous spectrum, i.e., the modulation of $\hat{q}_1(\xi)$ and $\hat{q}_2(\xi)$, respectively. The energy of a signal obtained by modulation of $\hat{q}_1(\xi)$ is given by

$$E=\int_{-\infty}^{\infty}|q(t)|^2\,dt=\frac{1}{\pi}\int_{-\infty}^{\infty}\log\left(1+\left|\hat{q}_1(\xi)\right|^2\right)d\xi=\frac{1}{\pi}\int_{-\infty}^{\infty}\log\left(1+\mathrm{A}^2\left|\psi(\xi)\right|^2\right)d\xi. \tag{16}$$

As soon as the absolute value of the carrier waveform can be lower bounded by some rectangle, the energy will go to infinity for $\mathrm{A}\to\infty$. The same holds for the modulation of $\hat{q}_2(\xi)$, which has been especially designed to enable explicit control the pulse energy.

3. The improved b-modulator

3.1 Carrier waveform

In light of the discussion in the previous section, we find that the carrier waveform should at least fulfill the following two conditions: $\psi(\xi)$ should have a

i) compactly supported $\Psi(\tau)$ to ensure finite pulse durations; and

ii) large enough MCE to enable sufficiently high signal energies.

The sinc and raised cosine carriers used for b-modulation so far satisfy these conditions, but there is nevertheless an issue with them that has not been obvious so far since we focused on the single carrier case until now. Ideally, the maximum energy we can achieve with a multicarrier system containing $2N+1$ carriers would be $(2N+1)\mathrm{MCE}[\psi]$. However, when performing b-modulation with sinc or raised cosine carriers, the individual carriers are only guaranteed not to influence each other at the carrier centers due to the Nyquist property. At other nonlinear frequencies, the individual carriers do interact and can form a maximum at random nonlinear frequencies that is very hard to control. Since the amplification factor has to satisfy $\mathrm{A}<1/\sup_{\xi}|b(\xi)|$, such an uncontrollable maximum can limit the maximum energy in a multicarrier system to random value much less that $(2N+1)\mathrm{MCE}[\psi]$. To avoid this issue, we require our carrier waveform to fulfill a third condition: $\psi(\xi)$ should be

Optics EXPRESS

iii) localized in the ξ domain so that with reasonably large carrier spacing ξ_s, no uncontrollable maxima occur in $|b(\xi)|$.

To address all three conditions i)—iii), we propose to use Fourier-transformed flat top windows (e.g., [20]) as carrier waveforms since they are bandlimited, concentrated in the ξ domain, and approximate a rectangle at their center (which has infinite MCE). In our experiments and simulations, we used the carrier that corresponds to the flat-top window

$$\Psi_{\text{flat top}}(\tau)=\frac{1}{T}\sum_{m=0}^{15}\mathrm{a_m}\,r\left(\frac{\tau}{T}\right)\cos\left(\frac{\pi\tau}{T}m\right),\qquad r(\tau)=\begin{cases}1, \textit{ if } |\tau|\le 1\\ 0, \textit{ otherwise}\end{cases}, \tag{17}$$

which was designed using the "Program 1" Matlab script in [20] with inputs that put equal weight on the perfect flatness of the carrier around zero and the decay of the sidelobes (i.e., $N=64$, $M=15$, $DN=D0=7$ and $delt=0$). The constant $T>0$ is the desired pulse duration in normalized units (see Section 2.3). The coefficients a_m are given as Table 1.

Table 1. The value of coefficients a_m

$a_0=1.00781249999087$	$a_4=2.01557690160615$	$a_8=1.80756640511884$	$a_{12}=0.229897459751809$
$a_1=2.01562499996723$	$a_5=2.01459671013285$	$a_9=1.49055821347783$	$a_{13}=0.064961507923051$
$a_2=2.01562499848123$	$a_6=2.00542418293614$	$a_{10}=1.03117157326193$	$a_{14}=0.0112874144984265$
$a_3=2.01562428510123$	$a_7=1.95813292084616$	$a_{11}=0.563957100582878$	$a_{15}=0.000905697614069561$

The corresponding carrier waveform is

$$\psi_{\textit{flat top}}(\xi)=\sum_{m=0}^{15}\mathrm{a_m}\left(\mathrm{sinc}\left(\frac{\xi T}{\pi}-m\right)+\mathrm{sinc}\left(\frac{\xi T}{\pi}+m\right)\right). \tag{18}$$

Both are shown as Fig. 1 for the duration $T=4.5$.

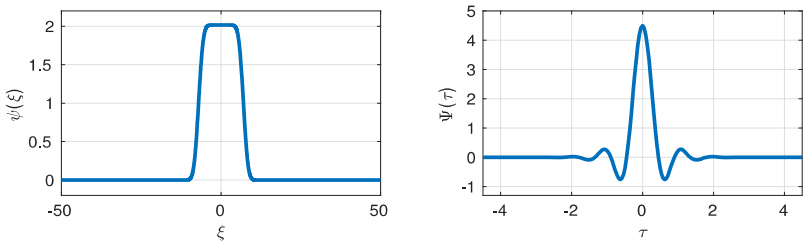

Fig. 1. The shape of the carrier $\psi(\xi)$ and its inverse Fourier transform $\Psi(\tau)$ for $T=4.5$.

3.2 Constellation shaping

The energy of the fiber input in the original b-modulation method $b(\xi)=\mathrm{A}u(\xi)$ with $u(\xi)$ as in (4) was adjusted through the power control factor $\mathrm{A}>0$. The energy of a single carrier that has been modulated with a symbol $\mathrm{s_n}\in\mathcal{A}$ is, as above,

$$\mathrm{E}[\mathrm{s_n}]=-\frac{1}{\pi}\int_{-\infty}^{\infty}\log\left(1-\mathrm{A}^2|s_n|^2\left|\psi(\xi)^2\right|\right)d\xi. \tag{19}$$

Optics EXPRESS

A disadvantage of the original b-modulation method discussed earlier is that the energy ratio $\mathrm{E}[\mathrm{s_n}]/\mathrm{E}[\mathrm{s_k}]$ for two different carriers $\mathrm{n} \neq \mathrm{k}$ can be very different from the energy ratio $|\mathrm{s_n}|^2/|s_k|^2$ of their symbols. This is in contrast to the linear case, where the ratios are equal. To avoid the generation of disproportionately weak carriers, we propose to abandon the power control factor $\mathrm{A} > 0$ and use a reshaped version

$$\mathcal{A}^{\mathrm{shaped}} = \{\mathrm{a}_1^{\mathrm{shaped}}, \ldots, \mathrm{a}_\mathrm{M}^{\mathrm{shaped}}\} \tag{20}$$

of the given modulation alphabet $\mathcal{A} = \{\mathrm{a}_1, \ldots, \mathrm{a}_\mathrm{M}\}$ instead.

In the improved b-modulator, a block of symbols $\mathrm{s}_{-\mathrm{N}}, \ldots, s_N \in \mathcal{A}$ is modulated as follows. Denote the index of the value in the alphabet that $\mathrm{s_n}$ takes by $\mathrm{m(n)}$ such that $\mathrm{s_n} = a_{m(n)}$. The $b(\xi)$ for the given block of symbols is then given by

$$b(\xi) = \sum_{\mathrm{m}=-\mathrm{N}}^{\mathrm{N}} s_n^{\mathrm{shaped}} \Psi(\xi - n\xi_s), \quad \text{where} \quad s_n^{\mathrm{shaped}} := \mathrm{a}_{\mathrm{m(n)}}^{\mathrm{shaped}} \in \mathcal{A}^{\mathrm{shaped}}. \tag{21}$$

The reshaped modulation alphabet is chosen as

$$\mathrm{a}_\mathrm{m}^{\mathrm{shaped}} := \sqrt{\gamma_\mathrm{m}}\, a_m, \quad \text{where} \quad \gamma_\mathrm{m} > 0. \tag{22}$$

Let $\mathrm{E_d} > 0$ denote some desired average energy (in normalized units). Assuming that $\mathrm{MCE}[\Psi]$ is high enough to support $\mathrm{E_d}$, the γ_m are defined indirectly by the relations

$$\mathrm{E}\left[\mathrm{a}_\mathrm{m}^{\mathrm{shaped}}\right] := -\frac{1}{\pi}\int_{-\infty}^{\infty} \log\left(1 - \gamma_m |a_m|^2 |\psi(\xi)|^2\right) d\xi = \frac{|a_m|^2}{\left(|a_1|^2 + \ldots + |a_M|^2\right)/M}\mathrm{E_d}, \tag{23}$$

where $\mathrm{m} = 1, \ldots, M$. The term in the middle of this equation is monotonously increasing in γ_m, while the right-hand side is known and independent of γ_m. Therefore, we could determine the γ_m using the bisection method; the integral was computed numerically. Note that our choice of γ_m ensures that the energy ratios of the modulated carriers match the energy ratios of their symbols with respect to the original modulation alphabet, i.e.,

$$\mathrm{E}\left[s_n^{shaped}\right] / E\left[s_k^{shaped}\right] = |s_n|^2 / |s_k|^2. \tag{24}$$

In other words, the generation of disproportionately weak carriers is avoided. Another advantage is that the average modulated carrier energy matches the desired average energy,

$$\frac{\mathrm{E}\left[\mathrm{a}_1^{\mathrm{shaped}}\right] + \ldots + \mathrm{E}\left[\mathrm{a}_\mathrm{M}^{\mathrm{shaped}}\right]}{M} = \mathrm{E_d}. \tag{25}$$

The γ_m are monotonously increasing functions of the desired energy $\mathrm{E_d}$. As $\mathrm{E_d}$ approaches the maximum carrier energy $\mathrm{MCE}[\psi]$, the γ_m will converge towards $1/\sup_\xi |a_m|^2 |\psi(\xi)|^2$.

3.3 Simulation examples

In this subsection, we numerically investigate the performance of the improved b-modulator with that of several other methods in a back-to-back (B2B) scenario. The original modulation alphabet is a 16-QAM. It is shown together with its shaped version, for a desired carrier energy $\mathrm{E_d} = 4$, in Fig. 2(a). The fiber inputs generated by the original b-modulator (i.e.,

Optics EXPRESS

$b(\xi) = \mathrm{A}u(\xi)$; A is adapted to control the signal energy; the constellation is not shaped), the improved b-modulator (i.e., $b(\xi) = u(\xi)$; the reshaped constellation is used to control the average signal energy) and the two conventional modulators (from $\hat{q}_1(\xi)$, $\hat{q}_2(\xi)$ mentioned in Section 2.2) all contain $2N+1=9$ flat-top subcarriers with random symbols and a shift of $\xi_s = 15$. We emphasize that in our setup *both* b-modulators, original and improved, use the same flat-top carrier. The reason for not using a sinc or the impulse response of a raised cosine was that, with such carriers, the original b-modulation scheme was not able to match the energies of the improved b-modulator. The advantage of this choice is that we can isolate the effect of constellation shaping in our investigations. Some example pulses are shown in Fig. 2(b). The symbol duration for the b-modulators is $T = 4.5$. For the $\hat{q}$-modulation methods, much larger windows are used to generate the initial signals and then truncated to $T = 4.5$. All four $q(t)$ have the same energy. The $q(t)$ generated by the b-modulators are constrained to [-2.25 2.25] by design, while the other $q(t)$ are more spread out and suffer from slowly decaying tails. The fiber inputs $q(t)$ generated by the b-modulators are exactly zero outside the interval [-2.25, 2.25], but they are already very small for $|t| > 1$. This phenomenon can be explained with the shape that the inverse Fourier transform $\Psi(\tau)$ of the carrier waveform $\psi(\xi)$ (see Fig. 1). It decays quickly and is very small long before it becomes exactly zero. Consequently, the same holds for the inverse Fourier transform $B(\tau)$ of $b(\xi)$, which in turn is at least indicative for the behavior of $q(t)$; for signals with low amplitudes $b(\xi)$ reduces to a conventional linear Fourier transform so that $B(\tau)$ reduces to $q(t)$. Hence, we will later be able to truncate the signals generated by the b-modulators to durations shorter than $T = 4.5$. The truncation error made will be much lower than for conventional $\hat{q}$-modulation because the tail is rapidly, and not slowly, decaying to zero. To corroborate this claim, we show the 99.9% durations and bandwidths of each $q(t)$ modulated with randomly chosen blocks of symbols by the four methods in Fig. 2(c). It can be seen that the 99.9% durations of the pulses generated by the b-modulators are consistently lower than that for the conventional modulation methods. Figure 2(d) shows the (conventional) Fourier transforms of the four fiber input types, which are all very similar.

Optics EXPRESS

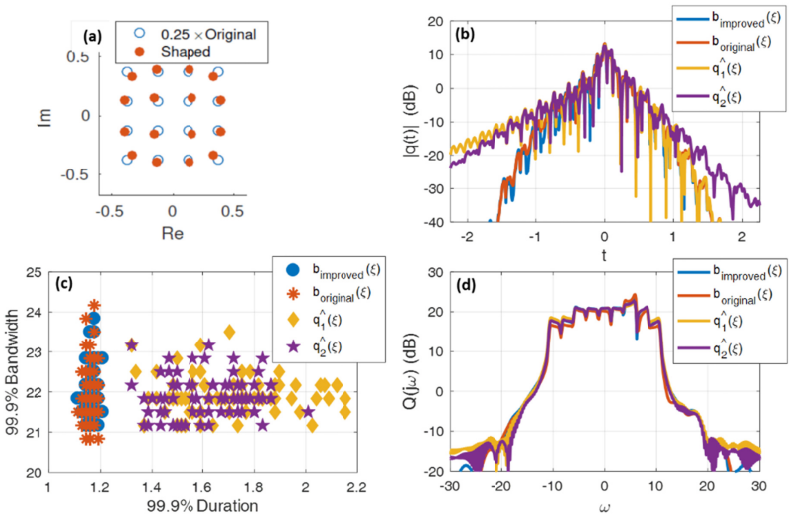

Fig. 2. (a) Constellation shape of 16 QAM and its shaped version with $E_d = 4$; (b) Time domain shape of the fiber inputs $|q(t)|$ generated by the improved b-modulator, original b-modulator, two conventional modulators by $\hat{q}_{1/2}$ with same information; (c) 99.9% durations and bandwidths of fiber inputs $q(t)$ by the four modulation methods; (d) Fourier transform spectra for the four fiber inputs $q(t)$.

Then, to understand the signal-noise interaction through NFT processing, we numerically investigated the back-to-back (B2B) performance of the signals generated by the four methods (described in the Sections 2.2, 2.3 and 3) under different normalized SNR (averaged time waveform power to averaged noised power ratio). We also investigated the performance of a linear frequency division multiplexing (FDM) scheme that uses the same flat-top carriers as the other methods. The pulses were truncated to a duration of $T = 2$ before transmission, where the impact of tail truncation is negligible for the b-modulation methods and the linear FDM method. No additional guard interval (GI) was used. For an average energy $E_d = 4$, the BER as a function of SNR for the four modulation methods are shown in Fig. 3(a). At a BER of 1e-3 (FEC threshold), the SNR penalties of the $\hat{q}_{1/2}$ modulation schemes and the original b-modulation method are ~6 dB and ~1 dB respectively in comparison with the linear FDM curve, while almost no penalty is observed for the improved b-modulation scheme. Since both b-modulation schemes use the same flat-top carriers and carrier spacing in this example, we attribute the better performance of the improved scheme to the use of reshaped constellation instead of a power control factor. The results clearly indicate that the b-modulation schemes are less sensitive to noises than the $\hat{q}_{1/2}$ -modulation schemes. A similar phenomenon has been observed for the discrete spectrum in [21] and the continuous spectrum in [17]. One possible explanation is that $a(\xi)$ is also affected by noise, such that the resulting effect encompasses an additional noise contribution. Another possible explanation is that a square 16-QAM constellation performs bad since additive white Gaussian noises (AWGN) in the time domain translate into quite complicated noises in the nonlinear Fourier domain. A sufficient theoretical understanding of how noises affect the nonlinear Fourier coefficients, which is required for the design of optimal constellations, is still lacking. In addition, for a fixed SNR = 8dB, the noise tolerance for the different methods under various average carrier energy E_d (which controls the average power of fiber inputs) are shown in Fig. 3(b). Higher desired carrier energies E_d lead to stronger decaying tails and less tolerance to noise for the

Optics EXPRESS

conventional non-linear methods. However, the improved b-modulator can largely reduce the sensitivity. The original b-modulator again performs worse than our improved version.

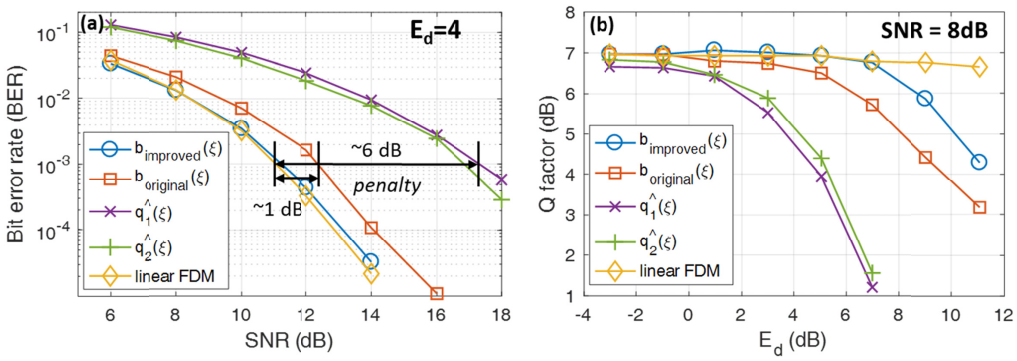

Fig. 3. For improved b-modulated, original b-modulated, $\hat{q}_{1/2}$ modulated and FDM systems in B2B scenario (a) BER vs SNR at an average energy of $E_d = 4$; (b) Q factor as function of average energy of E_d under SNR = 8dB.

3.4 The role of solitons

The b-modulators used here and in the literature so far generate signals that have no solitonic components. The question arises whether the addition of solitons could bring benefits to b-modulation. We suspect that these benefits are negligible.

It is well-known (see, e.g., [8]) that for finite-duration signals, the functions $a(\lambda)$ and $b(\lambda)$ can be found for any complex λ from their restrictions $a(\xi)$ and $b(\xi)$ with $\lambda = \xi$ real by using analytic continuation. The condition $a(\lambda)a^*(\lambda)^* + b(\lambda)b^*(\lambda) = 1$, which normally is only guaranteed for $\lambda = \xi$ real, consequently becomes true for all complex λ . Remember that solitons are represented in the NFT through eigenvalues λ_k , which now satisfy

$$a(\lambda_k) = 0 \Rightarrow b(\lambda)b^*(\lambda^*) = 1. \tag{26}$$

The signals generated by the b-modulator contain no solitons. It is known that solitons can be added on top of a time-limited signal without extending the temporal support, but from the equation above we see that the corresponding eigenvalues can only be added at the zeros of $1 - b(\lambda)b^*(\lambda^*)$. See, e.g., [22], [Sec. IV] or also [25], (Case c) in Sec. 3. The possible locations at which eigenvalues can be placed on top of a b-modulated signal thus depend on symbols $s_{-N}, \ldots, s_N$ that were used to generate $b(\xi)$. This seems to make it difficult to devise a practical modulation and demodulation scheme that uses solitons together with b-modulation.

4. Experimental results and discussion

4.1 Experimental setup

We also conducted experimental verifications of the proposed algorithm. Figure 4 shows the experimental setup and offline DSP structure. At the transmitter side, random 16-QAM symbols were mapped either onto the continuous spectrum $\hat{q}_{1/2}(\xi)$ or onto the scattering coefficient $b(\xi)$. The burst durations and the number of subcarriers were same as in the

Optics EXPRESS

simulation setting in Section 3.3, that is, the duration of the transmitted bursts was $T = 2$ and the number of subcarriers was $2N+1=9$. No extra zero guard interval (GI) was placed between neighboring bursts. After the inverse NFT, a linear pre-equalizer was used to compensate the imperfection of transmitter components. An arbitrary waveform generator (AWG) with 92 GSa/s was used to generate the electrical waveform of the burst train. With a normalization parameter $T_0 = 0.2$ *ns*, the burst duration in physical units is equal to $T \times T_0 =$ 0.4 *ns*. The total bit rate of the designed system is 14.4 Gbps. After conversion by the I/Q modulator, the optical waveform was amplified and launched into a fiber recirculating loop. The loop consists of two span 80-km SSMF and lumped amplification only by EDFA. A flat-top optical filter with a 3-dB bandwidth of 1 nm was used inside the loop to suppress the out-of-band amplified spontaneous emission (ASE) noise. Both the transmitter laser and local oscillator were from fiber laser sources with very low laser phase noise (NKT Koheras ADJUSTIK Fiber laser with linewidth < 100Hz). After alignment by a polarization controller in the x-polarization, the received signal was then coherently detected and sampled by a digital storage scope with a sampling rate of 80 GSa/s and a bandwidth of 33 GHz. The sampled signal was analyzed by off-line digital signal processing (DSP), whose structure is also shown in Fig. 4. After timing synchronization and frequency offset compensation, the received signal was separated into bursts for further NFT processing to recover the nonlinear spectrum. A training symbol based equalizer followed to compensate the impact of the channel distortion in NFDM systems. The last steps were symbol decision and bit error rate (BER) calculations.

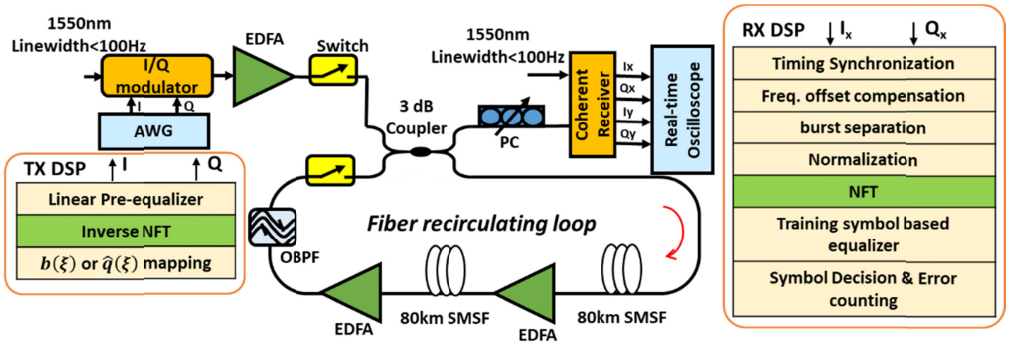

Fig. 4. DSP structure and experimental setup. AWG: arbitrary waveform generator; OBPF: optical band-pass filter; PC: polarization controller.

A development version of the software library FNFT [26] was used to compute the inverse and forward NFTs. The numerical algorithm that was used to compute the inverse NFT for the b-modulators is the modification of Algorithm 2 in [27] described in [16]. Note that this is a fast algorithm, which only requires $O(D\log^2 D)$ floating point operations (flops) in order to generate D samples of the signal $q(t)$. It will be part of the next release of FNFT. The algorithm for the NFT is already included in the current release of FNFT. It is fast as well and based on the results in [28]. The overall complexity of our transceiver digital signal processing is thus $O(D\log^2 D)$ flops, which is – not taking the hidden constants in the big-O notation into account – close to that of a conventional OFDM system.

4.2 Results and discussions

To illustrate the effectiveness of the proposed improved b-modulation scheme, we compared the performance of the different modulation systems in Fig. 5. A linear frequency division multiplexing (FDM) scheme that uses the same flat-top carriers and parameter setting as the other methods was also experimentally tested with the same setup platform. As shown in Fig.

Optics EXPRESS

5, after 640 km transmission, the improved b-modulated system offers 0.3 dB and 1.2 dB advantage in terms of Q-factor over the original b-modulated and FDM system. In addition, the improved b-modulated scheme extends the gain of nonlinear threshold (the optimum launched power) to ~4 dB in comparison to FDM system, while only 2 dB gain is observed for original b-modulated systems. This indicates the proposed b-modulation scheme can improve the tolerance to the fiber nonlinearity impairment. One will note that the results of $\hat{q}$ -modulated signals did not show the same advantages over FDM signals as in other NFDM demonstrations [23]. This is because $\hat{q}$ -modulated signals tend to have longer durations and slowly decaying tails in the time domain. In our system, where short time durations are enforced and no additional GI is used, they suffer from severe truncation errors. This further confirms the advantage of b-modulation in limiting the signal duration. We finally remark that signals designed using inverse NFTs are very sensitive to linear and nonlinear responses of optical transceivers [7,11]. Thus, our experimental results in Fig. 5 suffer from implementation penalties due to limitations of current practical devices, including linear and nonlinear responses, phase noise and limited resolutions of the optical transceivers. As a result, advanced modulation formats, digital signal processing, and calibration techniques will be important research topics and challenges for future NFT research.

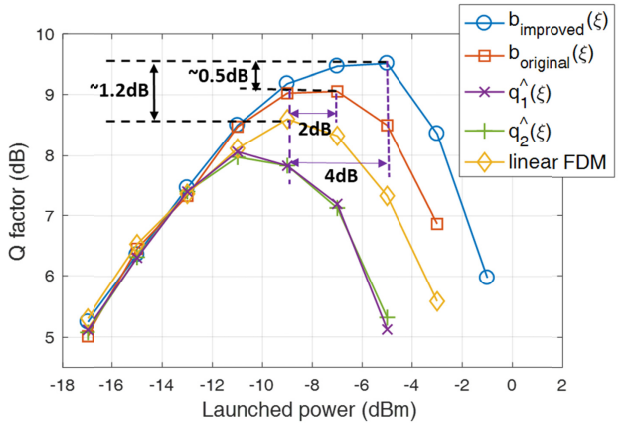

Fig. 5. Q-factor as function of average power at 640 km for improved b-modulated, original b-modulated, $\hat{q}_{1/2}$ modulated and linear FDM systems.

5. Conclusions

In this paper, we proposed to use flat top carriers and constellation shaping to improve on the recently proposed b-modulation scheme. The improved b-modulator provides better control over the signal power and avoids that some subcarriers are substantially weaker than others. Numerical studies and experimental demonstrations showed that these improvements translate into further reach and higher Q-factors. It was also demonstrated that b-modulation techniques allow one to generate pulses with lower time-bandwidth products than other continuous spectrum modulation methods. The proposed method serves as another step to further improve optical communications systems based on nonlinear Fourier transform.

Funding

European Research Council (ERC) under the European Union's Horizon 2020 research and innovation programme (grant agreement No 716669); The Hong Kong Government General Research Fund (PolyU 152116/15E).

Optics EXPRESS

References

1. E. G. Turitsyna and S. K. Turitsyn, "Digital signal processing based on inverse scattering transform," Opt. Lett. **38**(20), 4186–4188 (2013).
2. J. E. Prilepsky, S. A. Derevyanko, and S. K. Turitsyn, "Nonlinear spectral management: Linearization of the lossless fiber channel," Opt. Express **21**(20), 24344–24367 (2013).
3. J. E. Prilepsky, S. A. Derevyanko, K. J. Blow, I. Gabitov, and S. K. Turitsyn, "Nonlinear inverse synthesis and eigenvalue division multiplexing in optical fiber channels," Phys. Rev. Lett. **113**(1), 013901 (2014).
4. M. I. Yousefi and F. R. Kschischang, "Information transmission using the nonlinear Fourier transform, Part I: Mathematical tools," IEEE Trans. Inf. Theory **60**(7), 4312–4328 (2014).
5. M. I. Yousefi and F. R. Kschischang, "Information transmission using the nonlinear Fourier transform, Part II: Numerical methods," IEEE Trans. Inf. Theory **60**(7), 4329–4345 (2014).
6. M. I. Yousefi and F. R. Kschischang, "Information transmission using the nonlinear Fourier transform, Part III: Spectrum modulation," IEEE Trans. Inf. Theory **60**(7), 4346–4369 (2014).
7. S. K. Turitsyn, J. E. Prilepsky, S. T. Le, S. Wahls, L. L. Frumin, M. Kamalian, and S. A. Derevyanko, "Nonlinear Fourier transform for optical data processing and transmission: advances and perspectives," Optica **4**(3), 307–322 (2017).
8. M. J. Ablowitz, D. J. Kaup, A. C. Newell, and H. Segur, "The inverse scattering transform Fourier analysis for nonlinear problems," Stud. Appl. Math. **53**(4), 249–315 (1974).
9. A. Hasegawa and T. Nyu, "Eigenvalue communication," J. Lightwave Technol. **11**(3), 395–399 (1993).
10. T. Gui, C. Lu, A. P. T. Lau, and P. K. A. Wai, "High-order modulation on a single discrete eigenvalue for optical communications based on nonlinear Fourier transform," Opt. Express **25**(17), 20286–20297 (2017).
11. S. T. Le and H. Buelow, "64×0.5Gbaud nonlinear frequency division multiplexed transmissions with high order modulation formats," J. Lightwave Technol. **35**(17), 3692–3698 (2017).
12. V. Aref, S. T. Le, and H. Buelow, "Demonstration of fully nonlinear spectrum modulated system in the highly nonlinear optical transmission regime," *in Proceedings of European Conference on Optical Communication* (Institute of Electrical and Electronics Engineers, 2016), post deadline paper.
13. S. Wahls and H. V. Poor, "Fast numerical nonlinear Fourier transforms," IEEE Trans. Inf. Theory **61**(12), 6957–6974 (2015).
14. M. Kamalian, J. E. Prilepsky, S. T. Le, and S. K. Turitsyn, "Periodic nonlinear Fourier transform for fiber-optic communications, Part I: theory and numerical methods," Opt. Express **24**(16), 18353–18369 (2016).
15. M. Kamalian, J. E. Prilepsky, S. T. Le, and S. K. Turitsyn, "Periodic nonlinear Fourier transform for fiber-optic communications, Part II: eigenvalue communication," Opt. Express **24**(16), 18370–18381 (2016).
16. S. Wahls, "Generation of time-limited signals in the nonlinear Fourier domain via b-modulation," *in Proceedings of European Conference on Optical Communication* (Institute of Electrical and Electronics Engineers, 2017), paper W.3.C.6.
17. S. T. Le, K. Schuh, F. Buchali, and H. Buelow, "100 Gbps b-modulated nonlinear frequency division multiplexed transmission," in Optical Fiber Communication Conference (Optical Society of America, 2018), paper W1G.6.
18. X. Yangzhang, V. Aref, S. T. Le, H. Buelow, and P. Bayvel, "400 Gbps dual-polarisation non-linear frequency-division multiplexed transmission with b-modulation," Preprint arXiv:1806.10367 [eess.SP] (2018).
19. X. Yangzhang, M. I. Yousefi, A. Alvarado, D. Lavery, and P. Bayvel, "Nonlinear frequency-division multiplexing in the focusing regime," in Optical Fiber Communication Conference (Optical Society of America, 2017), paper Tu3D.1.
20. K. Duda, T. P. Zielinski, and S. H. Barczentewicz, "Perfectly flat-top and equiripple flat-top cosine windows," IEEE Trans. Instrum. Meas. **65**(7), 1558–1567 (2016).
21. T. Gui, T. H. Chan, C. Lu, A. P. T. Lau, and P. K. A. Wai, "Alternative decoding methods for optical communications based on nonlinear Fourier transform," J. Lightwave Technol. **35**(9), 1542–1550 (2017).
22. J. K. Brenne and J. Skaar, "Design of grating-assisted codirectional couplers with discrete inverse-scattering algorithms," J. Lightwave Technol. **21**(1), 254–263 (2003).
23. S. T. Le, V. Aref, and H. Buelow, "Combating the Kerr-nonlinearity limit with nonlinear signal multiplexing," *in Signal Processing in Photonic Communications* (Optical Society of America, 2018), paper SpM4G. 3.
24. J. C. Portinari, "An inverse scattering transform for potentials of compact support," J. Math. Phys. **19**(10), 2100–2102 (1978).
25. T. Aktosun, "Inverse scattering on the line with incomplete scattering data," Contemp. Math. **362**, 362 (2004).
26. S. Wahls, S. Chimmalgi, and P. J. Prins, "FNFT: a software library for computing nonlinear Fourier transforms," J. Open Source Software **3**(23), 597 1–11 (2018).
27. S. Wahls and V. Vaibhav, "Fast inverse nonlinear Fourier transforms for continuous spectra of Zakharov-Shabat type," Withdrawn Preprint arXiv:1607.01305v2 [cs.IT] (2016).
28. P. J. Prins and S. Wahls, "Higher order exponential splittings for the fast non-linear Fourier transform of the Korteweg-de Vries Equation," *in International Conference on Acoustics, Speech and Signal Processing* (Institute of Electrical and Electronics Engineers, 2018), paper SPTM-P9.4.